DOI: 10.6060/mhc256889k

Effects of Chlorine Substitution and Nanotube Oxidation on Ammonia Detection in Zinc Phthalocyanine-SWCNT Hybrid Sensors: Experimental Studies and Quantum Chemical Calculations

Victoria N. Ivanova,[a] Pavel O. Krasnov,[b] Alexander M. Makarenko,[a] Tamara V. Basova,[a] and Darya D. Klyamer[a@]

[a]*Nikolaev Institute of Inorganic Chemistry SB RAS, 630090 Novosibirsk, Russia*
[b]*International Research Center of Spectroscopy and Quantum Chemistry, Siberian Federal University, 660074 Krasnoyarsk, Russia*
[@]*Corresponding author E-mail: klyamer@niic.nsc.ru*

The development of highly sensitive and selective room-temperature ammonia sensors remains a critical challenge for environmental and biomedical applications. We report chemiresistive sensors based on hybrid materials formed by non-covalent functionalization of pristine and carboxylated single-walled carbon nanotubes (SWCNTs and SWCNT-COOH) with chlorinated zinc phthalocyanines, specifically, tetra- ($ZnPcCl_4$) and octa-chloro ($ZnPcCl_8$) derivatives and unsubstituted ZnPc for comparative purposes. Comprehensive characterization by FTIR, Raman spectroscopy and ICP-AES confirmed successful hybrid formation and revealed that oxidation of SWCNTs significantly enhances phthalocyanine loading via additional hydrogen-bonding interactions. All hybrid layers demonstrated reversible chemiresistive sensor response to NH_3 (1–50 ppm), with the highest performance observed for the hybrids with $ZnPcCl_4$. Notably, SWCNT-COOH/$ZnPcCl_4$ exhibited a 2–3-fold higher sensor response and a lower limit of detection (0.3 ppm) compared to the hybrids with pristine SWCNT (0.5 ppm), attributable to greater phthalocyanine coverage. Humidity and selectivity studies have revealed the following features: while SWCNT-COOH-based hybrids exhibit excellent sensitivity under dry conditions, their performance is affected by signal bias at high relative humidity (>40%). In contrast, SWCNT/$ZnPcCl_4$ maintains stable characteristics. These findings highlight the impact of phthalocyanine substitution and carbon nanotube type on sensor performance, providing a foundation for designing effective ammonia sensors.

Keywords: Hybrid materials, metal phthalocyanines, gas sensors, chemiresistive sensors, ammonia, DFT calculations.

Влияние хлор-замещения и окисления нанотрубок в гибридных сенсорах на аммиак на основе фталоцианинов цинка и SWCNT: экспериментальные исследования и квантово-химические расчеты

В. Н. Иванова,[a] П. О. Краснов,[b] А. М. Макаренко,[a] Т. В. Басова,[a] Д. Д. Клямер[a@]

[a]*Институт неорганической химии им. А.В. Николаева СО РАН, 6300900 Новосибирск, Россия*
[b]*Международный научно-исследовательский центр спектроскопии и квантовой химии Сибирского федерального университета, 660074 Красноярск, Россия*
[@]*E-mail: klyamer@niic.nsc.ru*

Разработка высокочувствительных и селективных датчиков на аммиак остается важной задачей для экологических и биомедицинских применений. В данной работе представлены адсорбционно-резистивные сенсоры на основе гибридных материалов, полученных нековалентной функционализацией исходных и карбоксилированных одностенных углеродных нанотрубок (SWCNT и SWCNT-COOH) хлор-замещенными фталоцианинами цинка – тетра- ($ZnPcCl_4$) и октахлорированными ($ZnPcCl_8$) производными, а также незамещённым фталоциани-

ном цинка (ZnPc) для сравнения. Комплексное исследование с использованием ИК- и КР-спектроскопии и элементного анализа подтвердило успешное образование гибридных материалов и показало, что окисление SWCNT значительно повышает содержание фталоцианина в гибридном материале за счет образования дополнительных водородных связей. Слои полученных гибридных материалов демонстрировали обратимый сенсорный отклик на NH_3 (1–50 ppm), причем наилучшие характеристики были достигнуты у гибридов с $ZnPcCl_4$. Обнаружено, что SWCNT-COOH/$ZnPcCl_4$ показал в 2–3 раза более высокий отклик и более низкий предел обнаружения (0,3 ppm) по сравнению с гибридными материалами на основе исходных SWCNT (0,5 ppm), что обусловлено более высоким содержанием фталоцианина в материале. Исследование влияния влажности и селективности на сенсорный отклик показало, что хотя гибриды на основе SWCNT-COOH демонстрируют высокую чувствительность при низкой влажности, их сигнал искажается при относительной влажности >40%. При этом SWCNT/$ZnPcCl_4$ сохраняет стабильные сенсорные характеристики. Полученные результаты демонстрируют, как молекулярная структура фталоцианина и тип нанотрубок влияют на чувствительность сенсора. Это открывает новые возможности для разработки высокопроизводительных датчиков аммиака.

Ключевые слова: Гибридные материалы, фталоцианины металлов, газовые сенсоры, адсорбционно-резистивные датчики, аммиак, квантово-химические расчеты.

Introduction

Recently, chemiresistive gas sensors have found wide application across diverse fields, including environmental monitoring, industrial safety, agriculture, and the food industry.[1–3] They are also increasingly employed in healthcare for the detection of disease-related biomarkers in exhaled breath and other biological fluids.[4] In pursuit of higher sensitivity, selectivity, and stability, researchers are actively exploring novel sensing materials. Among these, hybrid materials have garnered significant attention due to their synergistic and complementary properties. Carbon nanotubes (CNT) serve as excellent platforms for hybrid sensor design due to their large specific surface area and high conductivity.[5] To tailor their sensing performance, CNTs are often functionalized with a variety of compounds, including metal nanoparticles,[6] conjugated polymers,[7] and polyaromatic molecules.[8] Among the latter, metal phthalocyanines (MPc) are of particular interest due to their robust chemical stability, tunable electronic structure, and strong affinity for various gaseous analytes.

MPcs have been widely utilized in the development of chemiresistive sensors for detecting various gases.[9] Their physicochemical properties can be precisely engineered by modifying the phthalocyanine macrocycle - specifically, by varying the central metal ion, the type and number of substituents, and their positions in the aromatic ring.[10–12] This molecular-level tunability enables fine control over interactions with target gases.

To modify carbon nanotubes, phthalocyanines $MPcR_x$ (x = 4, 8, 16) with various substituents are used, among them R=*tert*-Bu,[13] -COOH,[14] F,[15] -$OCH(CH_2(OCH_2CH_2)_2O$-$CH_2CH_3)_2$,[16] -$OCH_2CH_2C(CH_3)_2$,[17–19] -$OCF_2CF_2CH_3$,[20] -$S(CH_2CH_2O)_3CH_3$) and pyrene[21,22] and some others. These hybrid materials are then used to create sensors for detecting gases, such as chlorine, nitrogen dioxide, and ammonia. This work focuses specifically on the development of ammonia sensors. Ammonia is a critical analyte in both industrial and biomedical contexts. Ammonia is produced in numerous biological and chemical processes, and its accurate monitoring is essential for assessing system efficiency, environmental compliance, and human health.[23]

Among the above list of publications several studies have reported the use of MPc-functionalized single-walled (SWCNTs) and multi-walled (MWCNTs) nanotubes in chemiresistive ammonia sensors.[13,16–19,21,22] In these systems, phthalocyanines bearing long alkyl or alkoxy chains are typically preferred due to their high solubility and strong non-covalent π–π interactions with CNT sidewalls, which facilitate the formation of stable dispersions and uniform thin films. Moreover, oxidized CNTs containing surface -COOH groups are often used to further enhance NH_3 sensitivity, as these functional groups promote stronger interactions with the basic ammonia molecule. For example, Sharma *et al.* [17] described the non-covalent functionalization of SWCNTs-COOH and MWCNTs-COOH with lead phthalocyanine ($PbPcR_4$, R= -$OCH_2CH_2C(CH_3)_2$). The hybrid PbPc/SWCNT-COOH and PbPc/MWCNT-COOH films showed a significantly stronger response to NH_3 compared to pristine nanotubes. While prior work has shown that oxidation of CNTs can improve their affinity for ammonia,[24,25] a direct comparative study of MPc-based hybrids derived from oxidized versus non-oxidized CNTs under identical experimental conditions has not yet been reported.

It has recently been demonstrated that the introduction of halogen (F, Cl) substituents into the phthalocyanine ring enhances the sensitivity of chemiresistive gas sensors to electron-donating gases like ammonia.[11] Due to the fluorination of phthalocyanine MPc, the molecular orbitals are closer to the Fermi level, which leads to an increase in the ionization potential and the electron affinity, which results in a more favorable acceptor behavior.[26] This makes halogenated MPcs particularly suitable for detecting reducing gases such as NH_3. At the same time, research on CNT hybrids functionalized with halogenated phthalocyanines remains limited. Notably, Sharma *et al.*[15] used $CuPcF_{16}$ to modify SWCNTs-COOH and MWCNTs-COOH, but evaluated their response only toward chlorine, which is an oxidizing gas, leaving their potential for ammonia sensing unexplored.

In this study, we synthesized hybrid materials by non-covalently functionalizing both pristine SWCNTs and carboxylated SWCNTs (SWCNT-COOH) with chlorinated zinc phthalocyanines: tetra-chloro ($ZnPcCl_4$) and octa-chloro ($ZnPcCl_8$) derivatives. For comparison, analogous hybrids with unsubstituted ZnPc were also prepared. The resulting materials were characterized using Fourier-transform infrared (FTIR) and Raman spectroscopy, and inductively coupled plasma atomic emission spectroscopy (ICP-AES) to quantify the phthalocyanine loading on the nanotube surfaces. Their chemiresistive responses to low concentrations of ammonia (1–50 ppm) were systematically evaluated at room temperature. To elucidate the origin of observed differences in sensor performance, quantum chemical calculations were performed. By correlating experimental sensing data with theoretical insights into adsorption energetics, this work aims to clarify how chlorine substituents in the phthalocyanine macroring and nanotube oxidation jointly influence ammonia sensitivity. Such understanding will guide the rational design of next-generation chemiresistive sensors with enhanced sensitivity, selectivity, and reliability for real-world applications.

Experimental

Materials and methods of characterization of hybrid materials

Unsubstituted ZnPc, along with chlorinated derivatives $ZnPcCl_4$ and $ZnPcCl_8$ (Figure 1), were synthesized and purified following literature procedure.[11] Single-walled carbon nanotubes (20770 – SWCNT Type 2, length 0.5–2.0 μm, OD 1.0–2.0 μm, assay 90%) were obtained from Sisco Research Laboratories Pvt. Ltd. (SRL) and used as received, without further purification.

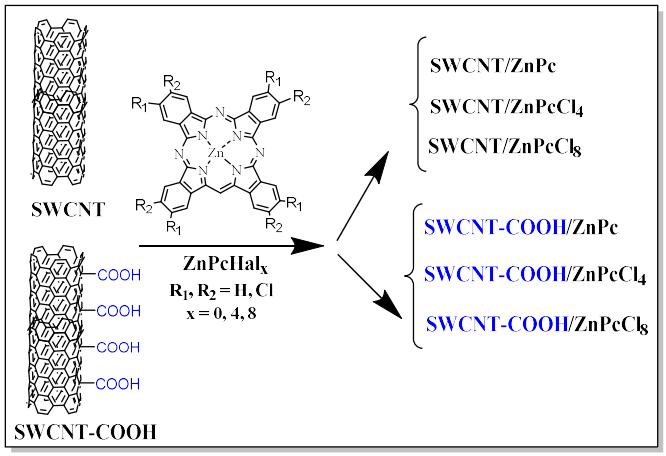

Figure 1. Scheme of the synthesis of hybrids material of SWCNT and SWCNT-COOH with chloro-substituted zinc phthalocyanines.

The resulting hybrid materials were characterized by Raman spectroscopy using a LabRAM Horiba spectrometer equipped with a 488 nm Ar^+ laser line, and by FTIR spectroscopy over the range of 650–4000 cm^{-1} on a FT-801 IR spectrometer. Zinc content in the hybrids was quantified via inductively coupled plasma atomic emission spectroscopy (ICP-AES) using a high-resolution spectrometer iCAP-6500 Duo (ThermoFisher Scientific, Waltham, MA). Samples were dissolved in concentrated sulfuric acid, and then diluted to 10 mL with deionized water prior to analysis. Instrumental parameters were set as follows: power supply 1150 W, nebulizer argon flow 0.70 $L{\cdot}min^{-1}$, auxiliary gas flow 0.50 $L{\cdot}min^{-1}$, and coolant gas flow 12 $L{\cdot}min^{-1}$.

Synthetic procedures

Synthesis of SWCNT-COOH. Oxidized carbon nanotubes (SWCNT-COOH) were prepared from commercially available SWCNTs. For this purpose, 5 mL of a 3:1 (v/v) mixture of concentrated HNO_3:H_2SO_4 (1.25 mL HNO_3 + 3.75 mL H_2SO_4) was added dropwise to 50 mg of SWCNTs while stirring. The reaction was conducted at 40 °C for 24 h. After that, the mixture was rinsed with distilled water until the p*H* reached approximately 7 and then dried at 100 °C.

Preparation of SWCNT/$ZnPcCl_x$ (x = 0, 4, 8). To perform non-covalent functionalization, a solution of zinc phthalocyanine ($ZnPcCl_x$, x = 0, 4 or 8) was added dropwise to a suspension of commercial SWCNTs in tetrahydrofuran (THF), under stirring conditions. The mixture was then subjected to ultrasonication for 60 min. After that, the solid product, SWCNT/$ZnPcCl_x$, was repeatedly centrifuged and washed with THF to remove any unreacted $ZnPcCl_x$.

Preparation of SWCNT-COOH/$ZnPcCl_x$ (x = 0, 4, 8). The hybrid material with oxidized carbon nanotube was prepared and purified similarly to SWCNT/$ZnPcCl_x$ material.

Investigation of sensor properties

The chemiresistive response of the hybrid layers to ammonia (10–50 ppm) was studied using a previously reported methodology.[27,28] The layers were deposited via spin-coating of 30 μL of suspensions of hybrids materials in dichloromethane (1 mg/mL) onto glass substrates with interdigitated platinum electrodes (DropSens, G-IDEPT10; gap dimension: 10 μm; cell constant: 0.0118 cm^{-1}). The rotation speed was 2000 r.p.m. The coated substrate was placed into a cell with an internal volume of 5 cm^3. Ammonia, diluted in air, was introduced into the cell for 30 s at a constant flow rate of 300 $mL{\cdot}min^{-1}$. The change in electrical resistance upon exposure to the gas analyte was measured using a Keithley 236 electrometer under a constant DC bias of 10 V. After each exposure, the cell was flushed with air until the layer's resistance returned to its baseline value before the next ammonia pulse was introduced. The relative sensor response (S_{resp}) was calculated using the formula: $S_{resp}=(R_i–R_0)/R_0$, where R_i is the resistance measured at a particular analyte concentration, and R_0 is the initial baseline resistance. Sensor response measurements were conducted at room temperature (20–25 °C) and relative humidity (RH) of 5–10%.

Theoretical calculations

The binding energies of zinc(II) phthalocyanine derivatives interacting with single-walled carbon nanotube CNT(10,0) used as a representative example of semiconducting carbon nanotubes and with NH_3 molecules adsorbed on these hybrid systems were calculated using the self-consistent charge density functional tight binding (SCC-DFTB) method. The computations were carried out within the DFTB+ software package [29,30], employing the 3OB parameter set (Slater-Koster files)[31,32] and incorporating dispersion corrections via the DFT-D3 scheme.[33,34] Charge transfer from ammonia to the hybrid structures was analyzed using Mulliken population analysis.[35,36] All electronic structure calculations were performed in a spin-unpolarized mode, as all investigated systems consisted solely of paired electrons.

Periodic boundary conditions were applied along the axis of the carbon nanotube. Each supercell comprised a segment of the nanotube with a length of 6*a*, where *a* denotes the unit cell length of CNT(10,0), and one macrocycle (MC) molecule adsorbed on

its surface. Based on our earlier findings,[37,38] the orientation of the macrocycle was selected to maximize π-orbital overlap between the macrocycle and the nanotube, corresponding to the most thermodynamically stable configuration. A vacuum spacing of 60 Å was introduced in the two directions perpendicular to the nanotube axis to eliminate artificial interactions between periodic images.

The Brillouin zone was sampled using a Monkhorst-Pack[39] grid of 1×1×25 *k*-points, with the nanotube aligned along the *z*-axis. Full structural optimization of both the hybrid systems and their ammonia adducts was conducted until the maximum force on any atom was reduced to 1×10^{-4} a.u.

The binding energy E_{b1} of each specific macrocycle (ZnPc, $ZnPcCl_4$, and $ZnPcCl_8$) with CNT(10,0) was estimated as the difference between the total energy of the entire hybrid structure (CNT(10,0)/MC) and the sum of the total energies of its isolated components (CNT(10,0) and MC):

$$E_{b1} = E_{\mathrm{CNT(10,0)/MC}} - E_{\mathrm{CNT(10,0)}} - E_{\mathrm{MC}}.$$

The average binding energy E_{b2} of an NH_3 molecule with each hybrid system was calculated analogously from the difference in total energies:

$$E_{b2} = \frac{1}{n}\left(E_{\mathrm{CNT(10,0)/MC}/n\mathrm{NH_3}} - E_{\mathrm{CNT(10,0)/MC}} - nE_{\mathrm{NH_3}}\right),$$

where *n* is the number of ammonia molecules. The effective charge acquired by the gas molecules was evaluated using the Mulliken population analysis scheme.[36,37]

Results and Discussion

Characterization of the hybrid materials

The prepared hybrids were analyzed using Raman and FTIR spectroscopy. In the IR spectra of materials containing carboxyl groups (SWCNT-COOH and SWCNT-COOH/$ZnPcCl_4$), characteristic C=O stretching vibrations from the -COOH group are observed at 1720–1740 cm^{-1}. The bands belonging to the vibrations of $ZnPcCl_4$ macrocycle are clearly visible in the spectrum of SWCNT-COOH/$ZnPcCl_4$ hybrid. However, characteristic bands of $ZnPcCl_4$ are not clearly observed in the SWCNT/$ZnPcCl_4$ due to its small amount.

Raman spectroscopy was used to analyze the functionalization of SWCNTs and SWCNT-COOH through the adsorption of $ZnPcHal_x$ derivatives onto their surfaces. Raman spectra of all hybrids, pristine SWCNTs, and oxidized SWCNT-COOH are shown in Figure 2. The D and G bands, characteristic vibrational modes of carbon nanotubes, were observed at approximately 1343 and 1590 cm^{-1}, respectively, in all spectra. The ratio of D and G band intensities (I_D/I_G) is a crucial parameter used to assess defect density in pristine nanotubes and monitor the quality of nanotubes as well as the modification of their surfaces by various molecules and functional groups. The I_D/I_G ratio was 0.021 in the case of pristine SWCNT, while in the case of hybrids it ranged from 0.022 to 0.033. This relatively minor change in I_D/I_G ratios is due to non-covalent character of interactions between $ZnPcHal_x$ molecules and nanotube surfaces. In addition to the vibrations typical of nanotubes, the spectra of the hybrids also contain bands corresponding to the vibrations of the $ZnPcHal_x$ macroring (see inset in Figure 2a,b).

The amount of zinc phthalocyanine ($ZnPcHal_x$) on the surface of SWCNT and SWCNT-COOH was quantified using inductively coupled plasma atomic emission spectroscopy (ICP-AES) by determining the zinc content in the hybrid material (Table 1). For SWCNT-based hybrids, the amount of adsorbed ZnPc, expressed as ν(MPc)/m(hybrid), was found to be 0.029±0.005, 0.038±0.004, and 0.009±0.001 mmol/g for SWCNT/ZnPc, SWCNT/$ZnPcCl_4$, and SWCNT/$ZnPcCl_8$, respectively. For hybrids based on oxidized nanotubes, the adsorbed amount of ZnPc derivatives was higher: 0.090±0.009, 0.096±0.010, and 0.057±0.006 mmol/g for SWCNT-COOH/ZnPc, SWCNT-COOH/$ZnPcCl_4$, and SWCNT-COOH/$ZnPcCl_8$, respectively.

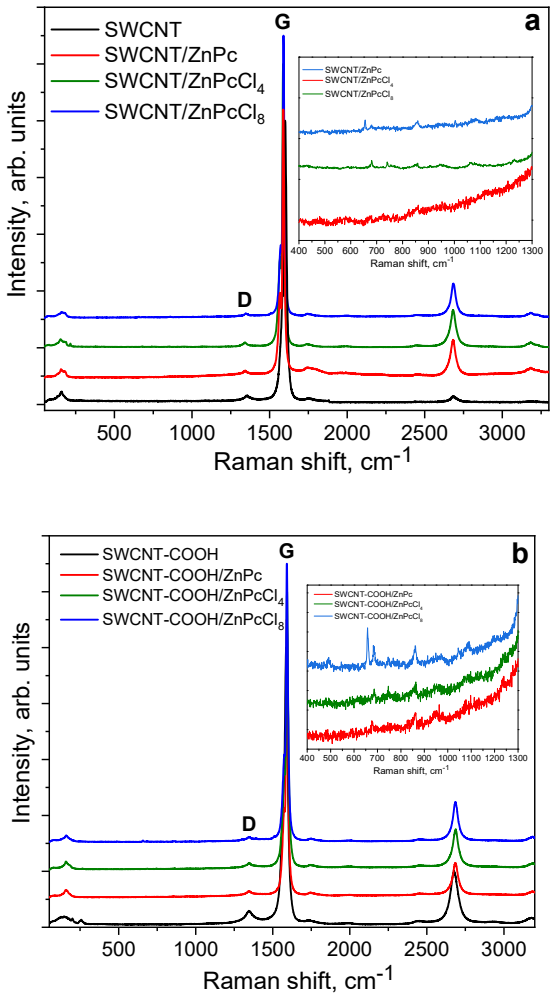

Figure 2. Raman spectra of pristine SWCNTs and their hybrid materials with chloro-substituted zinc phthalocyanines (a). Raman spectra of SWCNT-COOH and their hybrid materials with chloro-substituted zinc phthalocyanines (b). The insets show the enlarged spectral range corresponding to the vibrations of the $ZnPcHal_x$ macroring.

We can see that the amount of adsorbed ZnPc, $ZnPcCl_4$ and $ZnPcCl_8$ on the surface of oxidized carbon nanotubes (SWCNT-COOH) is 2–6 times greater than on pristine (non-oxidized) SWCNTs. This enhancement arises from the introduction of oxygen-containing functional groups – primarily carboxylic (-COOH) and hydroxyl (-OH) – onto the nanotube surface during oxidation. These polar

groups significantly increase the surface hydrophilicity and provide additional anchoring sites that facilitate stronger non-covalent interactions (*e.g.*, hydrogen bonding, dipole-dipole interactions, and electrostatic forces) with the ZnPc molecules, thereby promoting higher adsorption.

Interestingly, despite exhibiting the highest binding energy among the three derivatives, $ZnPcCl_8$ shows the lowest surface coverage on both SWCNTs and SWCNTs-COOH. This apparent contradiction can be attributed to steric hindrance. The eight bulky chlorine substituents increase the molecular footprint of $ZnPcCl_8$, limiting how closely adjacent molecules can pack on the nanotube surface. As a result, fewer $ZnPcCl_8$ molecules can adsorb per unit area compared to less substituted ZnPc and $ZnPcCl_4$, even though each individual interaction may be energetically more favorable.

Binding energy of zinc phthalocyanines in the hybrids materials

Quantum-chemical calculations yielded models of hybrid structures CNT(10,0)/$ZnPcCl_x$ (Figure 3).

The results show that chlorination at peripheral positions of ZnPc – and increasing the number of chlorine atoms from 4 to 8 – enhances the absolute binding energy between the macrocycle and CNT(10,0) (Table 2). This trend does not agree with the experimental observations in the case of hybrids with $ZnPcCl_8$ (Table 1). This discrepancy arises due to the fact that quantum chemical calculations estimate the thermodynamic stability of the complex, but do not take into account kinetic barriers that may interfere with adsorption or functionalization. Moreover, an increase in the number of chlorine substituents makes the phthalocyanine molecule more voluminous, which can prevent its diffusion to the surface of the nanotube, exacerbate spatial difficulties when the molecules approach each other, thereby limiting the number of adsorbed molecules on the surface of the nanotube. Consequently, although the resulting complex is thermodynamically more stable, its formation may be kinetically difficult.

To evaluate the effect of nanotube oxidation on macrocycle binding, we considered a model of CNT(10,0) functionalized with two carboxyl groups – denoted CNT(10,0)-2COOH (Figure 4). This model serves as a simplified representation to illustrate why oxidation enhances the degree of functionalization with metal phthalocyanines. Calculations for CNT(10,0)-2COOH/$ZnPcCl_x$ hybrids show that, as with the pristine CNT(10,0), the absolute binding energy E_{b1} increases with the number of chlorine substituents (Table 2). Furthermore, binding to the oxidized nanotube is stronger than to the pristine one. This enhancement stems from additional hydrogen bonding between hydrogen atoms at non-peripheral positions of the phthalocyanine and oxygen atoms of the carboxyl groups. Thus, these additional interactions explain the experimentally observed higher functionalization degree of oxidized nanotubes (Table 1).

Table 1. Amount of $ZnPcHal_x$ in hybrid material (mmol/g).

	SWCNT/ZnPc	SWCNT/$ZnPcCl_4$	SWCNT/$ZnPcCl_8$	SWCNT-COOH/ZnPc	SWCNT-COOH/$ZnPcCl_4$	SWCNT-COOH/$ZnPcCl_8$
$\nu_{ZnPcHalx}/m_{weight}$	0.029±0.005	0.038±0.004	0.009±0.001	0.090±0.009	0.096±0.010	0.057±0.006

$\nu_{ZnPcHalx}/m_{weight} = [\omega/M_M]\cdot 1000$, where $\nu_{ZnPcHalx}/m_{weight}$ is the amount of $ZnPcCl_x$ in the hybrid material (mmol/g), ω is the M content in weight determined by the ICP-AES method (%), M_M is the molar mass (g/mol).

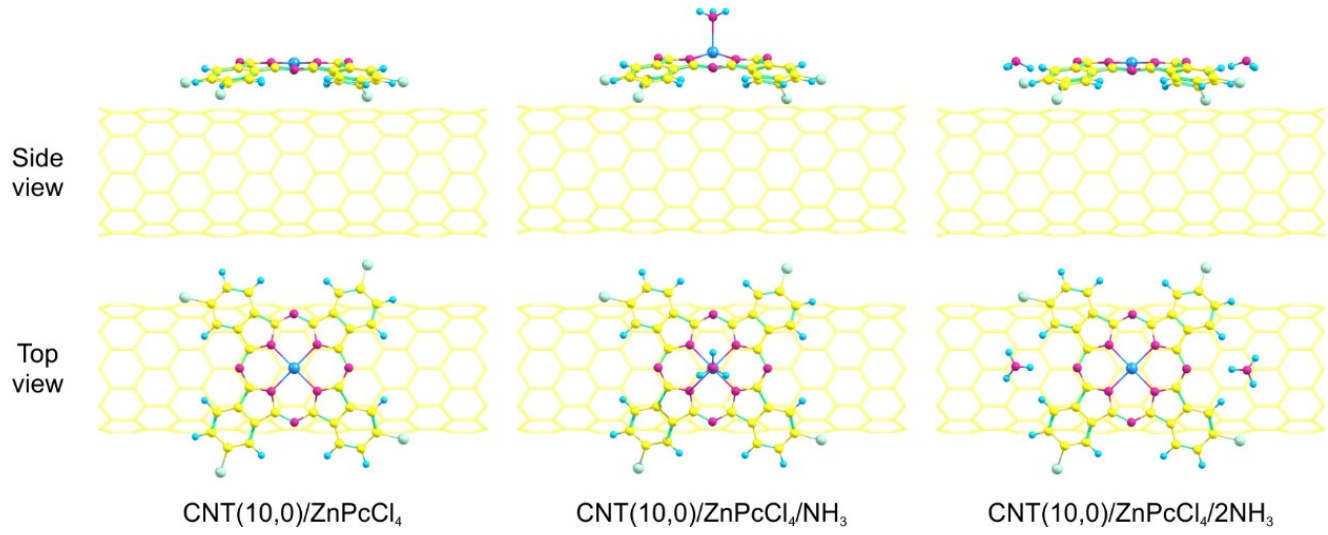

Figure 3. Optimized hybrid structures of the CNT(10,0) with $ZnPcCl_4$ and NH_3 molecules.

Table 2. Binding parameters of zinc phthalocyanines with CNT(10,0) and CNT(10,0)-2COOH, and binding parameters of ammonia with the resulting hybrid compounds.

Hybrids	E_{b1}, eV	+NH_3 (CB)		+2NH_3 (NCB)	
		E_{b2}, eV	q, e	E_{b2}, eV	q, e
CNT(10,0)/ZnPc	–1.866	–0.843	0.2310	–0.202	0.0040
CNT(10,0)/$ZnPcCl_4$	–2.189	–0.875	0.2360	–0.208	0.0076
CNT(10,0)/$ZnPcCl_8$	–2.520	–0.882	0.2381	–0.215	0.0091
CNT(10,0)-2COOH/ZnPc	–1.971	–0.840	0.2312	–0.203	0.0037
CNT(10,0)-2COOH/$ZnPcCl_4$	–2.569	–0.864	0.2354	–0.209	0.0051
CNT(10,0)-2COOH/$ZnPcCl_8$	–2.920	–0.877	0.2381	–0.216	0.0061

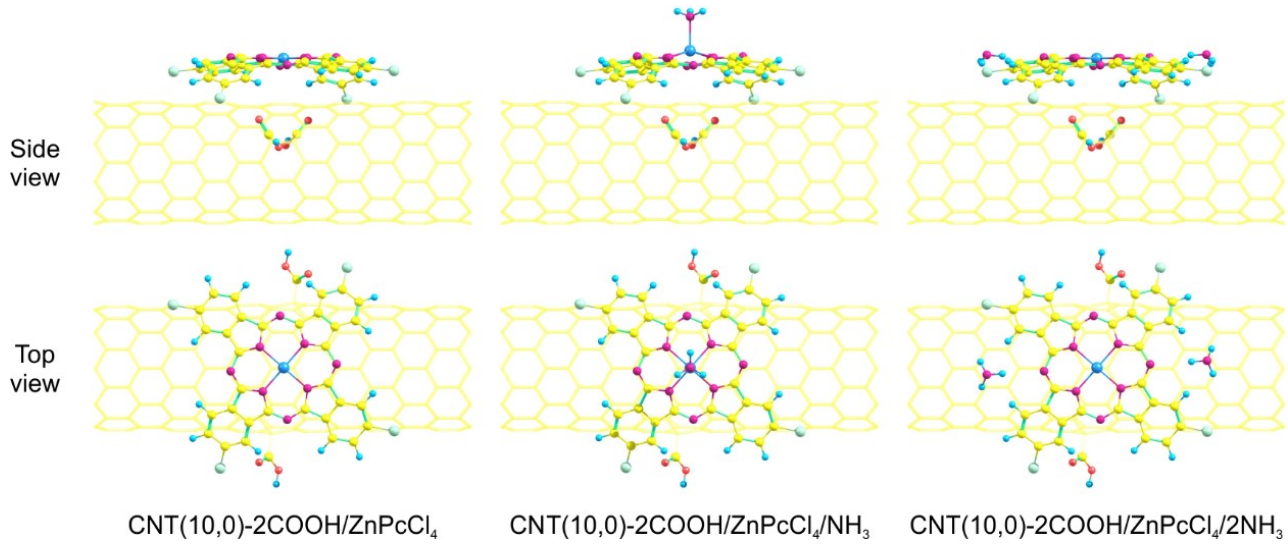

Figure 4. Optimized hybrid structures of the CNT(10,0)-2COOH with $ZnPcCl_4$ and NH_3 molecules.

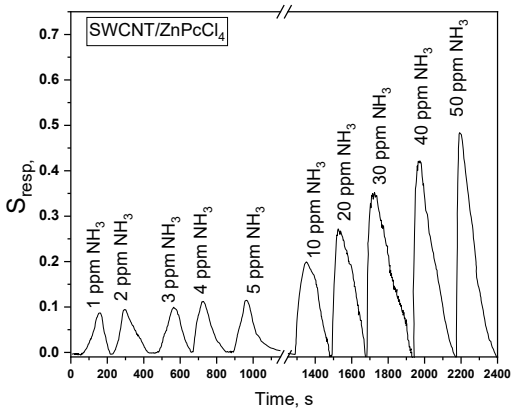

Figure 5. Relative sensor response of thin layers of SWCNT/$ZnPcCl_4$ toward NH_3 (1–50 ppm) measured at 23 °C and RH 10%.

Sensor properties of the hybrid layers

To reveal the effect of the number of chlorine substituents and the type of carbon nanotubes, the chemiresistive sensor response of all prepared hybrids to gaseous ammonia.

As illustrated in Figure 5 for the SWCNT/$ZnPcCl_4$ hybrid, all tested materials exhibited a rapid and reversible increase in electrical resistance upon exposure to ammonia. Following NH_3 introduction and subsequent purging of the chamber with dry air, the resistance fully recovered to its baseline value, confirming the reversibility of the sensing process at room temperature. The typical values of the initial base resistance (R_0) for SWCNT and SWCNT-COOH-based hybrids were in the range of 2.1–2.5·10⁴ Ohm.

The dependence of sensor response of SWCNT/$ZnPcCl_x$ and SWCNT-COOH/$ZnPcCl_x$ on ammonia concentration is given in Figure 6. Data from five replicate samples were used to calculate the standard deviation. The highest sensor response to ammonia was observed for layers of hybrid materials SWCNT/ZnPc and SWCNT/$ZnPcCl_4$, which correlated with the higher content of zinc phthalocyanine in these hybrids. A similar trend was observed for hybrids based on oxidized single-walled carbon nanotubes (SWCNT-COOH): the strongest responses were again recorded for ZnPc- and $ZnPcCl_4$-functionalized systems. In contrast, hybrids incorporating octachlorinated zinc phthalocyanine ($ZnPcCl_8$) consistently showed the lowest sensor response.

Notably, hybrid layers based on oxidized nanotubes SWCNT-COOH exhibited sensor responses 2–3 times greater than those based on pristine SWCNTs. This enhancement is attributed to the greater number of zinc phthalocyanine molecules anchored on the carboxylated nanotube surface, facilitated by stronger interactions.

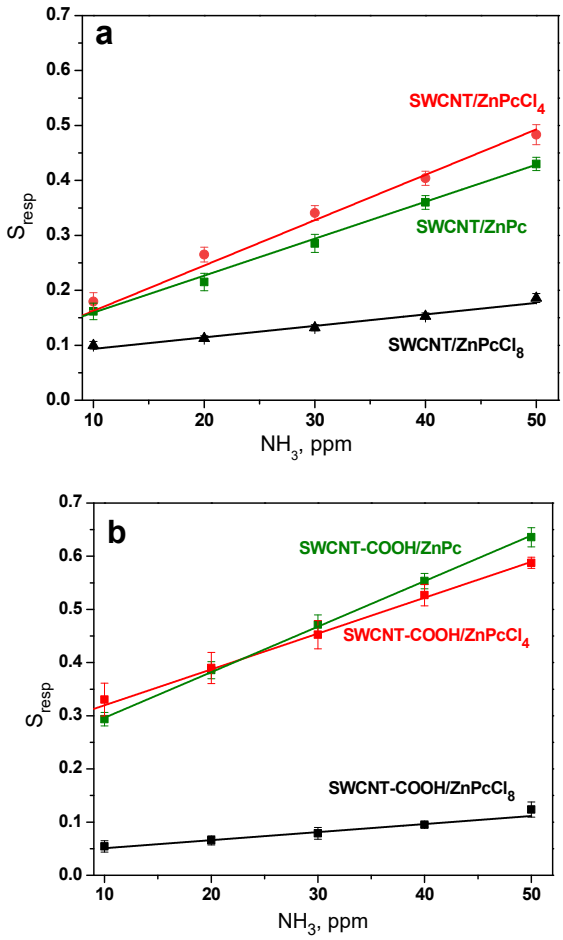

Figure 6. Dependence of the sensor response of the layers of SWCNT and SWCNT/ZnPc, SWCNT/$ZnPcCl_4$, SWCNT/$ZnPcCl_8$ hybrid materials (a) and SWCNT-COOH, SWCNT-COOH/ZnPc, SWCNT-COOH/$ZnPcCl_4$, SWCNT-COOH/$ZnPcCl_8$ (b) on NH_3 concentration (10–50 ppm). The dependencies were measured at 23 °C and RH 10%.

To support this claim, DFT calculations of ammonia adsorption on the hybrids were performed. Two distinct adsorption sites for NH_3 molecules have been previously identified on these hybrids: the central zinc atom, where NH_3 binds via covalent coordination (CB),[39] and the bridging nitrogen atoms of the phthalocyanine macrocycle, which facilitate non-covalent binding (NCB) through weak hydrogen bonds.[40,41] The NCB mode is considered more favorable for sensing applications, as the weaker interactions enable reversible adsorption and desorption – critical for reversible sensor response. Moreover, in this configuration, NH_3 molecules also interact directly with the carbon nanotube surface, thereby modulating the hybrid's electrical conductivity. In contrast, covalent coordination to the metal center impedes NH_3 desorption, leading to an irreversible sensor response.

We investigated both adsorption modes (Figures 3 and 4). Given the inherently weak nature of NCB interactions - and the correspondingly subtle electronic effects – we modeled the NCB configuration with two NH_3 molecules to amplify the observable response. As expected, the absolute binding energy for NH_3 coordinated to the zinc atom is more than four times greater than that for binding via the bridging nitrogen atoms (Table 2). Regardless of the binding mode, a consistent trend emerges: increasing the number of chlorine substituents on the phthalocyanine ring enhances both the absolute binding energy E_{b2} and the positive charge q acquired by NH_3 upon electron transfer to the hybrid system. This trend holds for both pristine CNT(10,0) and CNT(10,0)-2COOH hybrids.

Interestingly, while carboxyl functionalization strengthens the anchoring of the phthalocyanine macrocycle to the nanotube, it reduces the amount of charge transferred from NH_3 to the hybrid structure – an effect that would, in isolation, be expected to diminish sensor performance in oxidized systems compared to pristine ones. However, experimental results show the opposite: oxidized hybrids exhibit superior sensor responses. This apparent contradiction is resolved by considering the significantly higher degree of SWCNT functionalization achievable on oxidized nanotubes – an effect that compensates for the reduced charge transfer per ZnPc unit (see Tables 1 and 2). Consequently, the overall sensor response of hybrids based on oxidized SWCNTs surpasses that of their pristine counterparts.

Given their enhanced performance, SWCNT/$ZnPcCl_4$ and SWCNT-COOH/$ZnPcCl_4$ were selected for detailed characterization. Their sensor responses were evaluated across a broad NH_3 concentration range (1–50 ppm; Figure 7a). The limit of detection (LOD) was calculated using the standard formula: LOD = 3σ/m, where σ is the standard deviation of the sensor response to 1 ppm NH_3, and m is the slope of the linear region of the calibration curve. The resulting LODs were 0.5 ppm for SWCNT/$ZnPcCl_4$ and 0.3 ppm for SWCNT-COOH/$ZnPcCl_4$.

Response and recovery times were defined as the durations required to reach 90% of the maximum resistance change upon NH_3 exposure and to return to 90% of the baseline after purging with clean air, respectively (Figure 7b). At 1 ppm NH_3, the response/recovery times were 67 s/133 s for SWCNT/$ZnPcCl_4$ and 122 s/140 s for SWCNT-COOH/$ZnPcCl_4$.

The effect of operating temperature was examined by heating the sensing chamber to 40, 60, and 80 °C (Figure 8). As shown in Figure 9b, the response of SWCNT-COOH/$ZnPcCl_4$ decreased by approximately 1.5-fold as the temperature rose from 25 to 80 °C – a behavior consistent with physisorption, where increased thermal energy reduces gas adsorption on the solid surface.[42] In contrast, the response of the pristine SWCNT/$ZnPcCl_4$ hybrid remained nearly unchanged across the same temperature range (Figure 9a), suggesting a different interaction mechanism or greater thermal stability.

The influence of ambient humidity was also evaluated by varying the relative humidity (RH) in the test chamber from 5% to 70%, with RH monitored by a commercial hygrometer. The SWCNT-COOH/$ZnPcCl_4$ hybrid showed significant signal instability at relative humidities above 40%. This made it difficult to measure the sensor's response to ammonia at high humidity. This can be attributed to the strong hydrophilic nature of the -COOH and -OH surface groups, which leads to competition for water adsorption and a shift in the baseline. The response of SWCNT/$ZnPcCl_4$ was more stable at high humidity. For SWCNT/$ZnPcCl_4$, the value of sensor response to NH_3 increased by approximately 1.5 times at a relative humidity of 70% (Figure 9).

This may be due to the fact that water, like ammonia, acts as an electron donor, which can lead to an increase in the overall sensor response.

Selectivity was assessed by exposing the sensors to various analytes (Figure 10). Both hybrids showed significantly higher responses to NH_3 compared to CO_2 and common volatile organic compounds (VOCs). However, NO_2 emerged as a notable interferent, particularly for the oxidized nanotube system, where the response to 0.5 ppm NO_2 was ~10 times greater than that to NH_3, likely due to the presence of –COOH/–OH groups enhancing NO_2 adsorption.

Finally, the performance metrics of SWCNT/$ZnPcCl_4$ and SWCNT-COOH/$ZnPcCl_4$ were benchmarked against other carbon nanomaterial-based sensors functionalized with metal phthalocyanines (Table 3), highlighting their competitive sensitivity, speed, and selectivity for ammonia detection.

Conclusions

In this work, we report on chemiresistive sensors based on hybrid materials formed by non-covalent functionalization of pristine and oxidized single-walled carbon nanotubes (SWCNTs and SWCNT-COOH) with chlorinated zinc phthalocyanines, specifically, tetra- ($ZnPcCl_4$) and

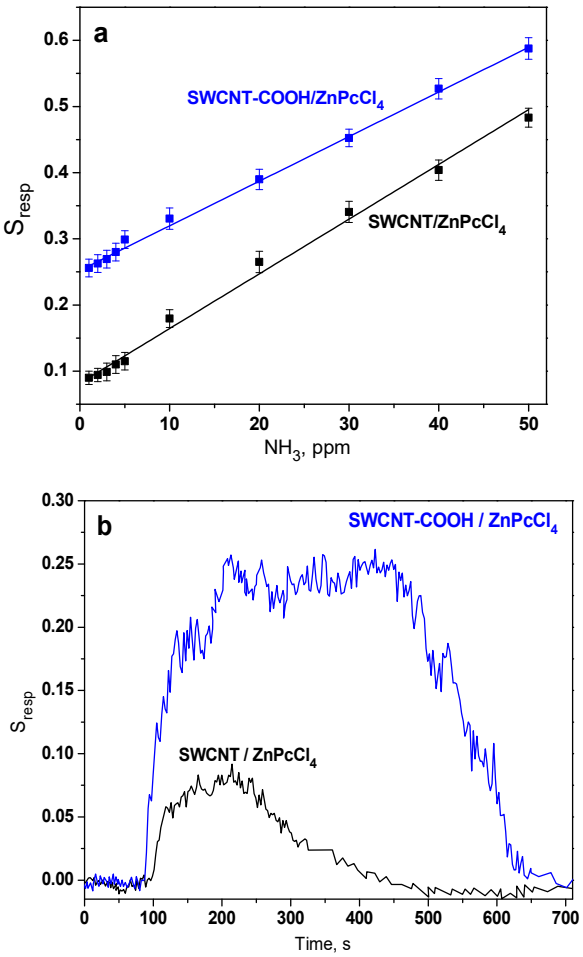

Figure 7. a – Dependence of the sensor response of the layers SWCNT/$ZnPcCl_4$ and SWCNT-COOH/$ZnPcCl_4$ on NH_3 concentration (1–50 ppm). b – Relative sensor response of the SWCNT/$ZnPcCl_4$ and SWCNT-COOH/$ZnPcCl_4$ to 1 ppm NH_3.

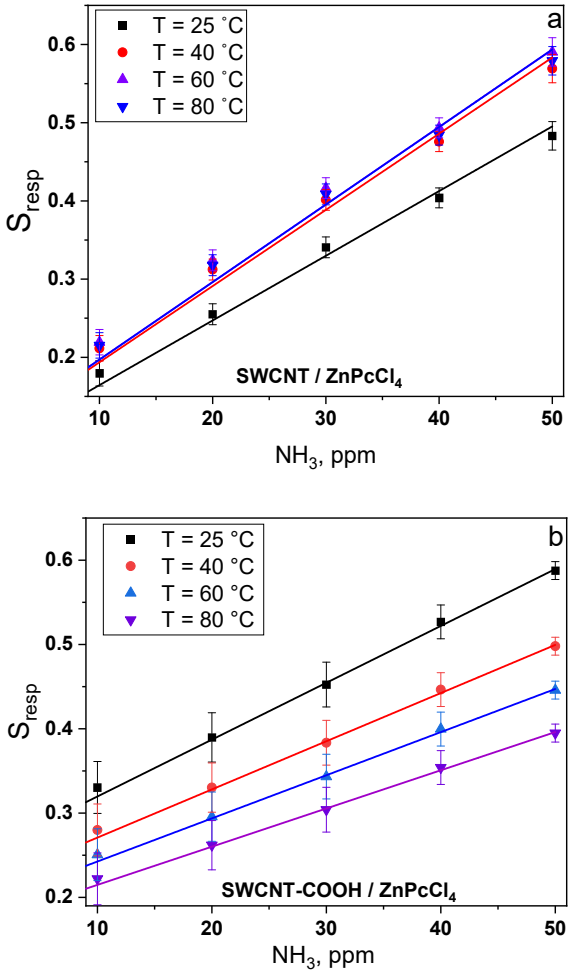

Figure 8. Temperature dependence of the sensor response of the hybrids SWCNT/$ZnPcCl_4$ (a) and SWCNT-COOH/$ZnPcCl_4$ (b) toward NH_3 (10–50 ppm).

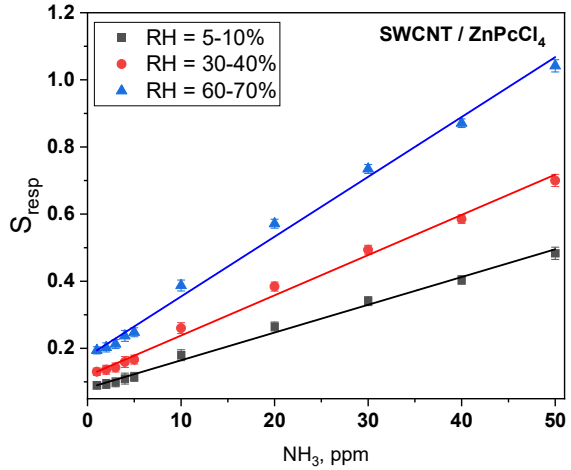

Figure 9. Dependence of the sensor response of the hybrids SWCNT/$ZnPcCl_4$ toward NH_3 measured at different RH.

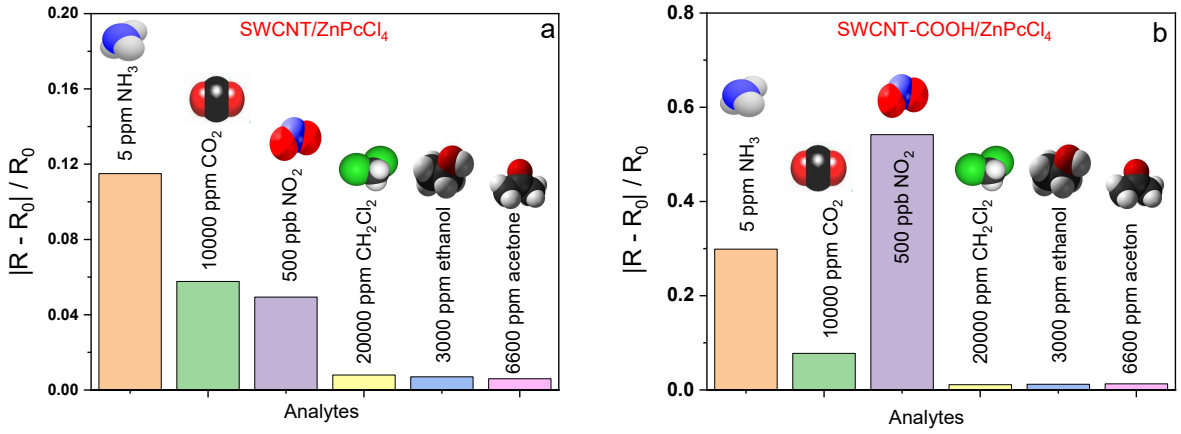

Figure 10. Sensor response of SWCNT/ZnPcCl4 (a) and SWCNT-COOH/$ZnPcCl_4$ (b) films to NH_3 (5 ppm), CO_2 (10000 ppm), NO_2 (0,5 ppm), dichloromethane (20000 ppm), ethanol (3000 ppm) and acetone (6600 ppm).

Table 3. Characteristics of sensors based on carbon nanomaterials functionalized with metal phthalocyanine derivatives.

Sensing layer	Linear concentration range, ppm	Response/recovery time, s	LOD, ppm	Ref.
CuTSPc@3D-(N)GF/PEDOT-PSS	1–1000	138 / 62 (200 ppm)	1	[43]
TFPCoPc/MWCNT	0.1–200	46/450 (50 ppm)	0.060	[44]
CuPc-3/MWCNTs	0.6–80	360 / 175 (2.5 ppm)	0.075	[19]
PbPc/SWCNT-COOH	2.5–20	n/a	0.150	[17]
SWCNT/$ZnPcCl_4$	1–50	67 / 133 (1 ppm)	0.5	This work
SWCNT-COOH/$ZnPcCl_4$	1–50	122 / 140 (1 ppm)	0.3	This work

octa-chloro ($ZnPcCl_8$) derivatives and unsubstituted ZnPc for comparative purposes. It was shown that the hybrid materials based on SWCNT-COOH demonstrated the higher chemiresistive sensor response than the hybrids based on pristine SWCNT. The key factor responsible for their enhanced sensor response is the higher degree of functionalization of SWCNT-COOH. This is enabled by additional hydrogen bonding between carboxyl oxygen atoms and non-peripheral hydrogen atoms of the phthalocyanine macrocycle. Gas sensing tests demonstrated that all hybrid layers demonstrated reversible chemiresistive sensor response to NH_3 (1–50 ppm) at room temperature, with the highest performance observed for the hybrids with $ZnPcCl_4$. SWCNT-COOH/$ZnPcCl_4$ exhibited a 2–3-fold higher sensor response and a lower limit of detection (0.3 ppm) compared to the hybrids with pristine SWCNT (0.5 ppm). Humidity and selectivity studies have revealed the following features: while SWCNT-COOH-based hybrids exhibit excellent sensitivity under dry conditions, their performance is effected by signal bias at high relative humidity (>40%). In contrast, SWCNT/$ZnPcCl_4$ maintains stable characteristics. These findings highlight the impact of phthalocyanine substitution and carbon nanotube type on sensor performance, providing a foundation for designing more effective ammonia sensors.

Funding. The study was funded by the Russian Science Foundation (project No 24-73-10058).

Acknowledgements. Authors are grateful to the Ministry of Science and Higher Education of the Russian Federation for the access to the computational cluster.

Author Contribution. Victoria Ivanova: methodology, formal analysis, investigation, writing – original draft, writing – review and editing. Pavel Krasnov: formal analysis, software, investigation, writing - original draft, visualization. Alexander Makarenko: formal analysis, investigation, validation. Tamara Basova: conceptualization, supervision methodology, validation, formal analysis, writing – original draft, writing – review and editing. Darya Klyamer: formal analysis, investigation, writing – original draft, writing – review and editing, project administration, fundung acquisition.

References

1. Fernández-Ramos M.D., Arenas-Martínez A., Pastrana-Martínez L.M., Cruz C., Pérez-Poyatos L.T., Morales-Torres S., Maldonado-Hódar F.J. *Microchem. J.* **2025**, *218*, 115291, doi: 10.1016/j.microc.2025.115291.
2 Park S.J., Lee S.M., Oh M.-H., Huh Y.S., Jang H.W. *Sustainable Food Technol.* **2024**, *2*, 266, doi: 10.1039/D3FB00196B.
3 Silva T.E.A.-R., Burisch F., Güntner A. T. *TrAC Trends in Anal. Chem.* **2024**, 177, 117790, doi: 10.1016/j.trac.2024.117790.
4 Landini N., Malagù C., Guidi V. *Sens. Actuat. B Chem.* **2022**, *371*, 132493, doi: 10.1016/j.snb.2022.132493.

5 Luo K., Peng H., Zhang B., Chen L., Zhang P., Peng Z., Fu X. *Coord. Chem. Rev.* **2024**, *518*, 216049, doi: 10.1016/j.ccr.2024.216049.
6 Dhall S., Sood K., Nathawat R. *Int. J. Hydrogen Energy* **2017**, *42*, 8392, doi: 10.1016/j.ccr.2024.216049.
7 Golovakhin V., Litvinova V.I., Manakhov A., Latypova A.R., Novgorodtseva O.N., Ukhina A.V., Ishchenko A.V., Al-Qasim A.S., Maksimovskiy E.A., Bannov A.G. *Mater. Today Commun.* **2024**, *39*, 109163, doi: 10.1016/j.mtcomm.2024.109163.
8 Oladipo M.E., Ogunsola S.S., Oladoye P.O. *Chemosphere* **2025**, *385*, 144549, doi: 10.1016/j.chemosphere.2025.144549.
9 Şahin Z., Meunier-Prest R., Dumoulin F., Kumar A., Isci Ü., Bouvet M. *Sens. Actuat. B Chem.* **2021**, *332*, 129505, doi: 10.1016/J.SNB.2021.129505.
10 Klyamer D., Bonegardt D., Basova T. *Chemosensors* **2021**, *9*, 133, doi: 10.3390/chemosensors9060133.
11 Bonegardt D., Klyamer D., Sukhikh A., Krasnov P., Popovetskiy P., Basova T. *Chemosensors* **2021**, *9*, 137, doi: 10.3390/chemosensors9060137.
12 Klyamer D., Bonegardt D., Krasnov P., Sukhikh A., Popovetskiy P., Basova T. *Chemosensors* **2022**, *10*, 515, doi: 10.3390/chemosensors10120515.
13 Polyakov M.S., Basova T.V. *Macroheterocycles* **2017**, *10*, 31, doi: 10.6060/mhc161176p.
14 Wu H., Chen Z., Zhang J., Wu F., He C., Wu Y., Ren Z., *J. Mater. Chem.* A **2017**, *5*, 24493, doi: 10.1039/C7TA07443C.
15 Sharma A.K., Mahajan A., Saini R., Bedi R.K., Kumar S., Debnath A.K., Aswal D.K. *Sens. Actuat. B Chem.* **2018**, *255*, 87, doi: 10.1016/j.snb.2017.08.013.
16 Polyakov M.S., Basova T.V., Göksel M., Şenocak A., Demirbaş E., Durmuş M., Kadem B., Hassan A. *Synth. Met.* **2017**, *227*, 78, doi: 10.1016/J.SYNTHMET.2017.02.024.
17 Wang B., Zhou X., Wu Y., Chen Z., He C. *Sens. Actuat. B Chem.* **2012**, *398*, 171–172, doi: 10.1016/j.snb.2012.04.084.
18 Wang B., Wu Y., Wang X., Chen Z., He C. *Sens. Actuat. B Chem.* **2014**, *190*, 157, doi: 10.1016/j.snb.2013.08.066.
19 Kang D., Wang B., Wang X., Li Y., Chen Z., He C., Wu Y., *Sens Actuat. B Chem.* **2017**, *246*, 262, doi: 10.1016/J.SNB.2017.02.083.
20 Liang X., Chen Z., Wu H., Guo L., He C., Wang B., Wu Y. *Carbon NY* **2014**, *80*, 268, doi: 10.1016/j.carbon.2014.08.065
21 Kaya E.N., Basova T., Polyakov M., Durmuş M., Kadem B., Hassan A. *RSC Adv.* **2015**, *5*, 91855, doi: 10.1039/c5ra18697h.
22 Kadem B., Göksel M., Şenocak A., Demirbaş E., Atilla D., Durmuş M., Basova T., Shanmugasundaram K., Hassan A. *Polyhedron* **2016**, *110*, 37, doi: 10.1016/J.POLY.2016.01.053.
23 Kwak D., Lei Y., Maric R. *Talanta* **2019**, *204*, 713, doi: 10.1016/j.talanta.2019.06.034.
24 Feng X., Irle S., Witek H., Morokuma K., Vidic R., Borguet E. *J. Am. Chem. Soc.* **2005**, *127*, 10533, doi: 10.1021/ja042998u.
25 Bannov A.G., Popov M.V., Brester A.E., Kurmashov P.B. *Micromachines* **2021**, *12*(2), 186, doi: 10.3390/mi12020186.
26 de Oteyza D.G., El-Sayed A., Garcia-Lastra J.M., Goiri E., Krauss T.N., Turak A., Barrena E., Dosch H., Zegenhagen J., Rubio A., Wakayama Y., Ortega J.E. *J. Chem. Phys.* **2010**, *133*, 214703, doi:10.1063/1.3509394.
27 Klyamer D., Bonegardt D., Basova T. *Chemosensors* **2021**, *9*, 133, doi: 10.3390/chemosensors9060133.
28 Ivanova V., Şenocak A., Klyamer D., Demirbas E., Makhseed S., Krasnov P., Basova T., Durmuş M. *Sens. Actuat. B Chem.* **2024**, *398*, 134733, doi: 10.1016/J.SNB.2023.134733.
29 Elstner M., Porezag D., Jungnickel G., Elsner J., Haugk M., Frauenheim T., Suhai S., Seifert G. *Phys. Rev. B* **1998**, *58*, 7260, doi: 10.1103/PhysRevB.58.7260.
30 Hourahine B., Aradi B., Blum V., Bonafé F., Buccheri A., Camacho C., Cevallos C., Deshaye M.Y., Dumitric T., Dominguez A., Ehlert S., Elstner M., Van Der Heide T., Hermann J., Irle S., Kranz J.J., Köhler C., Kowalczyk T., Kubař T., Lee I.S., Lutsker V., Maurer R.J., Min S.K., Mitchell I., Negre C., Niehaus T.A., Niklasson A.M.N., Page A.J., Pecchia A., Penazzi G., Persson M.P., Rezáč J., Sánchez C.G., Sternberg M., Stöhr M., Stuckenberg F., Tkatchenko A., Yu V.W.Z., Frauenheim T. *J. Chem. Phys.* **2020**, *152*, 124101, doi: 10.1063/1.5143190.
31 Lu X., Gaus M., Elstner M., Cui Q. *J. Phys. Chem. B* **2015**, *119*, 1062, doi: 10.1021/jp506557r.
32 Gaus M., Goez A., Elstner M. *J. Chem. Theory Comput.* **2013**, *9*, 338, doi: 10.1021/ct300849w.
33 Grimme S., Ehrlich S., Goerigk L. *J. Comput. Chem.* **2011**, *32*, 1456, doi: 10.1002/jcc.21759.
34 Grimme S., Antony J., Ehrlich S., Krieg H. *J. Chem. Phys.* **2010**, *132*, 154104. doi: 10.1063/1.3382344.
35 Mulliken R.S. *J. Chem. Phys.* **1955**, *23*, 1833, doi: 10.1063/1.1740588.
36 Mulliken R.S. *J. Chem. Phys.* **1955**, *23*, 1841, doi: 10.1063/1.1740589.
37 Krasnov P.O., Basova T.V., Hassan A. *Appl. Surf. Sci.* **2018**, *457*, 235, doi: 10.1016/J.APSUSC.2018.06.282.
38 Krasnov P.O., Ivanova V.N., Basova T.V. *Appl. Surf. Sci.* **2021**, *547*, 149172, doi: 10.1016/J.APSUSC.2021.149172.
39 Monkhorst H.J., Pack J.D. *Phys. Rev. B* **1976**, *13*, 5188. doi: 10.1103/PhysRevB.13.5188.
40 Krasnov P., Ivanova V., Klyamer D., Fedorov A., Basova T. *Chemosensors* **2022**, *10*, 479 doi: 10.3390/chemosensors 10110479.
41 Ivanova V., Klyamer D., Krasnov P., Kaya E. N., Kulu I., Tuncel Kostakoğlu S., Durmuş M., Basova T. *Sens. Actuat. B Chem.* **2023**, *375*, 132843, doi: 10.1016/J.SNB.2022.132843.
42 Rodrigues C.C., de Moraes D., da Nóbrega S.W., Barboza M.G. *Bioresour. Technol.* **2007**, *98*, 886, doi: 10.1016/j.biortech.2006.03.024.
43 Dehsari H.S., Gavgani J.N., Hasani A., Mahyari M., Shalamzari E.K., Salehi A., Taromi F.A. *RSC Adv.* **2015**, *5*, 79729, doi: 10.1039/C5RA13976G.
44 Liang X., Chen Z., Wu H., Guo L., He C., Wang B., Wu Y., *Carbon* **2014**, *80*, 268, doi: 10.1016/j.carbon.2014.08.065.

Received 21.11.2025
Accepted 17.12.2025